HHS Public Access

Author manuscript

Angiogenesis. Author manuscript; available in PMC 2023 August 01.

Published in final edited form as:

Angiogenesis. 2022 August ; 25(3): 397–410. doi:10.1007/s10456-022-09833-w.

Capillary Morphogenesis gene 2 (CMG2) mediates growth factor-induced angiogenesis by regulating endothelial cell chemotaxis

Lorna M. Cryan[b], **Tsz-Ming Tsang**[a], **Jessica Stiles**[b], **Lauren Bazinet**[b], **Sai Lun Lee**[a], **Samuel Garrard**[a,b], **Erika Madrian**[b], **Cody Roberts**[a], **Jessie Payne**[a], **Andrew Jensen**[a], **Arthur E. Frankel**[c], **P. Christine Ackroyd**[a], **Kenneth A. Christensen**[a], **Michael S. Rogers**[b,*]

[a]Department of Chemistry and Biochemistry, Brigham Young University, Provo, Utah, United States of America 84602.

[b]Department of Surgery, Vascular Biology Program, Children's Hospital Boston, Harvard Medical School, Boston, Massachusetts, United States of America 02115.

[c]Department of Medicine, West Palm Beach VA Medical Center, 7305 N Military Trail, West Palm Beach, FL, United States of America 33410

Abstract

Anthrax protective antigen (PA) is a potent inhibitor of pathological angiogenesis with an unknown mechanism. In anthrax intoxication, PA interacts with capillary morphogenesis gene 2 (CMG2) and tumor endothelial marker 8 (TEM8). Here we show that CMG2 mediates the antiangiogenic effects of PA and is required for growth-factor-induced chemotaxis. Using specific inhibitors of CMG2 and TEM8 interaction with natural ligand, as well as mice with the CMG2 or TEM8 transmembrane and intracellular domains disrupted, we demonstrate that inhibiting CMG2, but not TEM8 reduces growth-factor-induced angiogenesis in the cornea. Furthermore, the antiangiogenic effect of PA was abolished when the CMG2, but not the TEM8, gene was disrupted. Binding experiments demonstrated a broad ligand specificity for CMG2 among extracellular matrix (ECM) proteins. *Ex vivo* experiments demonstrated that CMG2 (but not TEM8) is required for PA activity in human dermal microvascular endothelial cell (HMVEC-d) network formation assays. Remarkably, blocking CMG2-ligand binding with PA or CRISPR knockout abolishes endothelial cell chemotaxis but not chemokinesis in microfluidic migration assays. These effects are phenocopied by Rho inhibition. Because CMG2 mediates the chemotactic response of endothelial cells to peptide growth factors in an ECM-dependent fashion, CMG2 is well-placed to integrate growth factor and ECM signals. Thus, CMG2 targeting is a novel way to inhibit angiogenesis.

[*]to whom correspondence should be addressed: Dr. Michael S. Rogers, 11.211 Karp Family Research Bldg., 300 Longwood Ave., Boston, MA 02115, michael.rogers@childrens.harvard.edu.

Disclosures: The authors have no competing interests.

Keywords

chemotaxis; chemokinesis; epithelial cell migration; angiogenesis; anthrax toxin; anthrax toxin receptor 2 (ANTXR2); capillary morphogenesis gene 2 (CMG2); anthrax toxin receptor 1 (ANTXR1); tumor endothelial cell marker 8 (TEM8)

Introduction

Pathological angiogenesis contributes to diseases as varied as cancer and corneal neovascularization [1]. Sprouting angiogenesis is induced by a wide variety of growth factors [1], and vessel growth is guided by endothelial cells migrating up a chemoattractant gradient [2]. These cells integrate a variety of chemotactic, haptotactic, and mechanical inputs to determine their migration direction [3]. The oriented movement of mesenchymal cell types (fibroblasts, neutrophils, etc.) in response to a solute gradient (chemotaxis) has been extensively studied. However, the mechanisms by which endothelial cells integrate chemotactic and haptotactic stimuli and orient themselves in a chemotactic gradient are less well understood.

We previously reported that anthrax protective antigen (PA) inhibits angiogenesis and tumor growth [4], but the receptor(s) and mechanism mediating this effect was unclear. Here, we report our discovery that capillary morphogenesis protein 2 (CMG2, aka the PA receptor ANTXR2) is a viable target for antiangiogenic therapy and that CMG2 targeting inhibits angiogenesis by specifically inhibiting the ability of endothelial cells to orient their migration toward a growth factor gradient. Knockout or inhibition of physiological ligand binding to CMG2 results in a significant reduction of corneal neovascularization, endothelial tube formation, and cell migration in response to a series of growth factors. Remarkably, we find that CMG2 blockade inhibits migration by randomizing the direction of endothelial cell migration without substantially affecting overall cell motility.

Results

Blockade of endothelial cell CMG2 inhibits corneal neovascularization.

PA^{SSSR} is a PA furin cleavage site mutant (RKKR→SSSR) that results in improved circulating half-life [5] and improved antiangiogenic activity [4]. We previously demonstrated that administration of either PA or PA^{SSSR} inhibits angiogenesis, as measured by endothelial cell migration, corneal neovascularization, and tumor growth [4]. PA^{SSSR} can interact with both anthrax toxin receptors at concentrations achieved by the doses administered. CMG2 has an affinity for PA of ~0.2nM [6] and TEM8 has an affinity ~10nM [7,8], while PA concentrations of 250nM are achieved by systemic dosing [7,5,9–11]. Because either of these interactions could cause the antiangiogenic effects of PA^{SSSR} *in vivo*, we performed a series of experiments to compare the relative contributions of CMG2 and TEM8 to corneal neovascularization in mice. First, we sought to disrupt ligand-receptor interaction using either CMG2-Fc or TEM8-Fc (extracellular domain fused to an antibody Fc domain) to block endogenous ligand [12,13]. In the corneal micropocket assay, administration of CMG2-Fc significantly inhibited basic fibroblast growth factor

(bFGF)-induced vessel growth compared to the untreated control, but the TEM8-Fc fusion did not (Figure 1A). We confirmed the relative importance of CMG2 vs. TEM8 in corneal angiogenesis by administering antibodies specific to either the CMG2 or TEM8 extracellular domains. The SR-8F7/C7 anti-CMG2 antibody [14] significantly reduced bFGF-induced corneal neovascularization in a dose-dependent manner (Figure 1B). In contrast, treatment with the anti-TEM8 antibody L2 at a dose and schedule previously shown to inhibit tumor growth in mice (20 mg/kg/q2d) [15] resulted in no significant decrease in corneal neovascularization compared to the vehicle control (Figure 1C). Together, these results show that blocking CMG2 significantly inhibits corneal angiogenesis, while blocking TEM8 does not.

To confirm the relative importance of CMG2 vs. TEM8 as a mediator of angiogenesis in the cornea, we next sought to identify phenotypic changes that result from loss of CMG2 or TEM8 transmembrane and intracellular domains as a result of transmembrane domain knockout [7]. Therefore, we performed the corneal micropocket assay in WT and CMG2-ΔTM-ICD ($CMG2^{-/-}$) mice, using either bFGF or VEGF to induce vessel growth (Figure 1D). $CMG2^{-/-}$ mice exhibit a striking reduction in both bFGF-induced (Figure 1E) and VEGF-induced (Figure 1F) corneal neovascularization versus WT mice, particularly in females (Figure S1A–B). Notably, female mice exhibit >85% reduction in VEGF response (Figure S1B). These results indicate a role for CMG2 in corneal angiogenesis. In contrast, TEM8-ΔTM-ICD ($TEM8^{-/-}$) mice exhibited no significant reduction when stimulated with VEGF (Figure 1H) and only modest reductions in bFGF-induced neovascularization (15%; $p<0.01$) (Figure 1G, S1C–D). These data confirm that CMG2 plays a substantial role in corneal neovascularization, while TEM8 plays only a modest role.

To exclude the possibility that a third anthrax toxin receptor might mediate the antiangiogenic effects of PA^{SSSR}, we measured the antiangiogenic activity of PA^{SSSR} in $CMG2^{-/-}$ or $TEM8^{-/-}$ mice. In $CMG2^{-/-}$ mice, PA^{SSSR} did not further reduce bFGF-induced corneal angiogenesis (Figure 2A). In contrast, PA^{SSSR} treatment significantly reduced corneal neovascularization in $TEM8^{-/-}$ mice (Figure 2B). Hence, we conclude that PA^{SSSR} exerts its antiangiogenic effects in the cornea by inhibiting CMG2.

To establish whether endothelial cells mediate the antiangiogenic effect of CMG2 disruption or blockade, we performed tube formation assays in Matrigel with human dermal microvascular endothelial cells (HMVEC-d), which express both CMG2 and TEM8. We compared the antiangiogenic effects of PA^{SSSR} on cells selectively expressing only one of the two receptors (Figure S2E). In TEM8 knockdown (KD) cells (which primarily express CMG2), PA^{SSSR} administration resulted in a concentration-dependent reduction in the extent of tube network formation (Figure S2F–G). In contrast, tube formation in CMG2 KD cells was not altered by PA treatment (Figure S2F–G), consistent with an earlier report that CMG2 knockdown decreases HUVEC tube formation [16]. Together with the whole-animal gene disruption data described above, these results demonstrate that CMG2, but not TEM8 expression, is required for the antiangiogenic activity of PA^{SSSR} and that the effects of PA^{SSSR} on endothelial cells correlate with whole-animal effects on angiogenesis. Thus, we conclude that CMG2 is the only target mediating the antiangiogenic effects of PA^{SSSR} in endothelial cells.

Disrupting the CMG2 transmembrane and intracellular domains results in altered vascular development in vivo.

Having demonstrated previously that CMG2 is vital for angiogenesis under two pathological conditions (*i.e.,* corneal neovascularization and tumor growth [4]), we next sought to determine how CMG2 disruption affects developmental angiogenesis. Since $CMG2^{-/-}$ animals have been shown to be generally healthy [17,7], we sought more subtle phenotypes. Therefore, we compared retinal vessel structures between WT and $CMG2^{-/-}$ mice to test for altered vessel development. The total vascular area was not measurably different between the two genotypes (Figure 3). However, the vascular growth pattern was subtly different between $CMG2^{-/-}$ and WT mice. Careful quantitation of these mouse retinas showed that while the total number of veins in the retina of WT and $CMG2^{-/-}$ mice is similar (Figure 3A–B), $CMG2^{-/-}$ mice have slightly fewer arteries (Figure 3A, C) and exhibit 2.5-fold more arteriolar branches than those of WT mice (Figure 3A, D). Hence, although CMG2 is not required for angiogenic development in the retina, CMG2 alters the pattern and appearance of the retinal vasculature.

CMG2 binds multiple ECM ligands.

In addition to anti-CMG2 antibodies and PA, both small molecules and peptides that compete with PA for CMG2 binding inhibit angiogenesis [18–22]. These data support the idea that PA^{SSSR} exerts its antiangiogenic effects *in vivo* by competing with interaction(s) between the (extracellular) CMG2 von Willebrand Factor A (vWA) [23,24] domain (including the metal ion-dependent adhesion site; MIDAS) [25,26] and endogenous ligand(s). However, the specific ligands that regulate angiogenesis by binding CMG2 remain unidentified. ECM proteins are likely candidates for CMG2 binding *in vivo* because of CMG2's homology with integrins [24], modest available data that shows CMG2 interaction with ECM proteins [27,14], and the observation that in individuals with hyaline fibromatosis syndrome (HFS), CMG2 mutations in the VWA domain result in widespread accumulation of extracellular matrix (ECM) proteins, including Col VI [14]. It has been proposed that CMG2 binds Col IV and fibronectin [27], or alternately, Col VI but not Col IV or fibronectin [14]. However, previous single-concentration assessment of CMG2 binding to different ECM materials cannot distinguish differences in affinity from differences in the number of binding sites attached to the assay substrate, making competing claims challenging to assess. We used ELISA to measure the CMG2 K_d for a series of different ECM proteins, including Col I, Col VI, laminin, and fibronectin (Figure S3). Consistent with a previous report [14], we find the highest maximum binding to collagen VI-coated wells.

In contrast, measurement of equilibrium binding affinity shows that each of the ECM proteins tested (collagen I, collagen VI, laminin, and fibronectin) interact with CMG2 with indistinguishable near-micromolar K_d values (Table 1). Both positive and negative control assays (CMG2 + PA^{SSSR} and CMG2 + PA^{SSSR} in the presence of EDTA, respectively) mirrored previously published K_d values [10]. The similar CMG2 affinity for the different matrix proteins tested indicates that CMG2 can bind to multiple ECM-derived sites. Such promiscuous binding of ECM proteins also indicates that, like integrins, CMG2 could play a significant role in cell adhesion and motility through direct interactions with multiple extracellular matrix components.

CMG2 mediates cell adhesion and migration ex vivo.

We next worked to illuminate the CMG2-mediated endothelial process that PA^{SSSR} disrupts to decrease angiogenesis. We have previously demonstrated that PA^{SSSR} affects transwell migration but not proliferation in HMVEC [4], a primary endothelial cell type. We confirmed that CMG2 knockdown in HMVEC-d did not significantly reduce proliferation (Figure S2A–D). Switching to the more genetically tractable immortal EA.hy926 endothelial cell line, we used CRISPR to target exon1 and isolated cell clones that exhibit loss of CMG2 uptake as measured by flow cytometry assay (Figure 4A, Figure S4). Concordant with our HMVEC-d results, in EA.hy926 cells, we observed that treatment with PA^{SSSR} did not affect cell proliferation (Figure 5A).

Having eliminated proliferation as the mediator of CMG2 targeting, we evaluated endothelial cell adhesion. CMG2 targeting using 200pM PA^{SSSR} significantly reduced EA.hy926 cell adhesion on plates coated with different ECMs (Collagens I, IV, and VI, Human Fibronectin, and Laminin-111), but not on BSA control plates (Figure 5B). Together, these data suggest that CMG2 plays a role in mediating cell adhesion to ECM proteins [24] and that PA^{SSSR} binding to CMG2 inhibits that phenotype.

A significant function of cell adhesion is to enable cell migration, and we have found that inhibition of HMVEC-d transwell migration *ex* vivo is a strong predictor of inhibition of angiogenesis *in vivo* (manuscript in preparation). Specifically, from a FRET screen [21,28] of 265,778 small molecules, we identified 26 compounds that bind CMG2 but not TEM8. All were tested for anti-proliferative and anti-migratory activity against HMVEC-d, *ex vivo*, and 19 for antiangiogenic activity *in vivo*. Additional analysis (Table 2) demonstrates that effects on migration strongly predict effects on angiogenesis. Together with results from knockout, natural products [19,18,22], and PA^{SSSR}, these results strongly demonstrate that CMG2-mediated effects on endothelial cell migration are critical to growth-factor-driven angiogenesis.

To dissect the nature of the effects of CMG2 inhibition on endothelial cell migration, we turned to a microfluidic migration assay that allows visualization of individual cells migrating in a stable growth factor gradient in real-time. First, we confirmed that PA^{SSSR} significantly reduces cell migration toward FBS on multiple different ECM substrates (Figure 5C–D), even at the 200pM concentration expected to result in only 50% bound CMG2. Specifically, we leveraged the microfluidic migration assay data to compare two different aspects of migration: total cell movement (chemokinesis) and directional motion towards growth-factor-containing serum (chemotaxis). Targeting CMG2 in EA.hy926 cells with PA^{SSSR} at the CMG2 K_d (200pM) resulted in a significant decrease in observed chemotaxis (e.g., 70% inhibition of chemotaxis on a serum-coated substrate, $P<0.01$; Figure 5C). In contrast, the total distance traveled by PA^{SSSR} treated cells was only modestly reduced (~20%) compared to untreated cells (Figure 5D). Thus, CMG2 targeting with PA^{SSSR} alters chemotaxis with little effect on chemokinesis.

Similarly, while CMG2 WT cells migrated toward serum (Figure 4B), $CMG2^{-/-}$ cells showed complete abolition of chemotaxis ($P<0.001$, Figure 4C,F) with an only slight alteration of chemokinesis (Figure 4G). To confirm that loss of chemotaxis in $CMG2^{-/-}$ cells

was not a consequence of off-target CRISPR effects, we complemented the CMG2 mutation with a vector expressing a fusion protein with the clover fluorescent protein fused to the carboxy-terminus of CMG2 (Figure 4D). We found that CMG2 add-back restored both PA^{SSSR} uptake (Figure 4A) and EA.hy926 cell chemotaxis (Figure 4D,F). Together, these data demonstrate that CMG2 knockout abolishes chemotaxis without substantially altering chemokinesis, a phenotype that echoes the effect of targeting CMG2 with PA^{SSSR}. Thus, CMG2 is a critical component of chemotactic response *ex vivo*, therefore, likely regulates endothelial cell chemotaxis *in vivo*.

CMG2 mediates chemotaxis in response to several key angiogenic growth factors

We have previously demonstrated that CMG2 targeting inhibits VEGF- and bFGF-induced corneal neovascularization (Rogers et al. [4]; Figure 1), and CMG2 knockdown has been reported to reduce migration of uterine cells towards PDGF-B [29]. Therefore, we evaluated the impact of CMG2 targeting on CMG2-mediated chemotaxis towards each of VEGF, bFGF, and PDGF, as well as a lipid endothelial chemoattractant, S1P. As shown in Figure 6 and Figure S5, EAhy.926 cell chemotaxis towards VEGF, bFGF, and PDGF, but not S1P, is dramatically inhibited by PA^{SSSR}, while chemokinesis is almost unchanged. Similar results were obtained in $CMG2^{-/-}$ cells, confirming that loss of directionality results from CMG2 loss of function rather than novel PA-induced signaling (Figure 6, Figure S5).

CMG2 mediation of endothelial cell chemotaxis and angiogenesis involves RhoA.

Microtubule orientation is the primary determinant of migration direction, and in developing zebrafish embryos, microtubule-based epiblast polarization is a RhoA-dependent process that requires CMG2. Based on these data, because RhoA is an established regulator of chemotaxis [30,31], and because coimmunoprecipitation data suggest complex formation between CMG2 and RhoA [32,33], we hypothesized that CMG2 and RhoA signal through the same pathway to regulate angiogenesis. Therefore, we sought to determine whether disruption of RhoA phenocopied the effect of CMG2 targeting on chemotaxis. As shown in Figure 6G–H and Figure S6A–B, treatment with the Rho inhibitor C3 exoenzyme abolishes EA.hy926 cells chemotaxis towards VEGF but has a minimal effect on chemokinesis. In contrast, S1P-induced chemotaxis was not altered by the presence of C3 exoenzyme (Figure 6A–B, Figure S6C–D). These data are consistent with the recent demonstration that RhoA knockdown abolishes HUVEC migration towards VEGF but not towards S1P [34]. Moreover, the retinal images presented by Zahra et al. (Figure 6C in Zahra et al. [34]) evince more branching in the primary arteriole of $RhoA^{-/-}$ mice vs. wild-type controls, a phenotype very reminiscent of our observations in $CMG2^{-/-}$ mice (Figure 4). Together, these data demonstrate a striking concordance between the effects of CMG2 targeting and RhoA targeting and suggest that CMG2 and RhoA fall in the same chemotaxis signaling pathway.

Discussion

Here we show that the antiangiogenic effects of PA^{SSSR} treatment result from inhibition of CMG2, which both disrupts cellular adhesion to ECM materials and causes cells to lose the ability to orient toward chemotactic cues from angiogenic growth factors. Indeed,

CMG2 targeting can altogether abolish Rho-A mediated directional migration towards at least three growth factors. However, this paper has important limitations. For example, although we know that CMG2 can interact with several ECM proteins, we don't know which of these interactions is key to supporting corneal angiogenesis. In addition, although Rho and CMG2 interact in other contexts [32,35] and the strong concordance between the phenotypes resulting from Rho and CMG2 blockade suggests that they share downstream signaling, we have not elucidated a detailed molecular mechanism by which CMG2 directs endothelial cell chemotaxis. As in the HeLa and zebrafish contexts, it may be that ligation of CMG2 by ECM ligand induces the release of a src-talin-vinculin-actin complex and recruitment of a src-Rho complex that then recruits Dia [35,32]. In zebrafish, these events orient the microtubule cytoskeleton [32], a process key to endothelial cell migration [36,37]. However, in the HeLa context, PA is an agonist of this process, while in endothelial cells PA antagonizes migration [4] indicating that CMG2 signaling in endothelial cells may differ substantially from that in HeLa cells. In addition, the mechanism by which CMG2 is involved in growth factor gradient sensing remains to be elucidated.

Notwithstanding these limitations, our data suggest that CMG2 is an attractive target for the development of antiangiogenic therapies. Notably, the bulk of existing antiangiogenic therapies target a single growth factor, VEGF, and its receptor and are subject to the development of drug resistance caused by the breakthrough of alternate angiogenic pathways [38–41]. However, since the development of resistance may be completely inhibited if at least three angiogenic pathways are inhibited [42], CMG2 targeting holds promise as a broad spectrum antiangiogenic therapeutic strategy that is less susceptible to the development of drug resistance than existing anti-VEGF therapy.

Methods

Corneal micropocket assay

The corneal micropocket assay was performed as described[43] using pellets containing 80 ng of basic fibroblast growth factor (bFGF) or 180 ng of human carrier-free recombinant vascular endothelial growth factor (VEGF; R&D Systems) in C57BL/6J mice (male and female adult (>8week old), Jackson Labs) or relevant knockout animals bred in-house. The treated groups received i.p. injections in PBS as indicated in the text. Specifically, Fc fusion proteins were given on day 1, antibodies were given on days 1 and 3, and PA was given daily, starting on day 0. Control mice received only vehicle i.p. The area of vascular response was assessed on the 5th (bFGF) or 6th (VEGF) postoperative day using a slit lamp. Typically, at least 10 eyes per group were measured. All animal experiments were performed in a blinded fashion under protocols approved by the Boston Children's Hospital Institutional Animal Care and Use Committee.

The CMG2-Fc and TEM8-Fc fusion proteins were a kind gift of Planet Biotechnology and were produced as described and exhibit affinity for ligand (PA) consistent with that of the parent receptor [12,13]. The SR-8F7/C7 is a rat IgG2a/kappa anti-murine-CMG2 antibody. Western blotting of murine colon extract with this antibody results in a single band at ~50kDa (the expected molecular weight) and only background reactivity in colon of knockout mice (Figure S7B). This antibody, together with western blot characterization data

were a kind gift of Gisou van der Goot and Laurence Abrami. The L2 anti-TEM8 antibody was a kind gift of Brad St. Croix and has been previously shown to bind and inhibit TEM8 interaction with ligand (PA) [15].

CMG2 and TEM8 KO mice

CMG2 and TEM8 ΔTM-ICD mice were a kind gift from Stephen Leppla. These mice have a deletion of transmembrane domain, resulting in loss of expression of both the transmembrane and intracellular domains [7]. They were housed in the ARCH facility at Boston Children's Hospital on standard food and bedding (CMG2) or on standard food and bedding, with supplemental soft food available (Nutra-gel mouse diet, Bio-Serv, Flemington, NJ). Genotyping was performed by Transnetyx (Cordova, TN).

Protein preparation

PA^{SSSR} and PA^{E733C} were expressed from pET-22b (RRID: Addgene 11079) into the periplasm and purified from the periplasmic lysate via anion exchange chromatography (Q-sepharose, GE Life Sciences Cat: 25236), using 20 mM Tris-HCl pH 8.0 with 20 mM NaCl (Buffer A) and Buffer A + 1 M NaCl. Endotoxin was removed by passing twice through polylysine coated cellulose beads (Thermo Fisher Cat: 88275), followed by an endotoxin test using the gel clot method and appropriate dilutions.

HMVEC proliferation assay

Human microvascular endothelial cells (Cambrex) were maintained in EGM-2 (Cambrex) according to the vendor's instructions and used before passage 7. On day 0, proliferating cultures of BCE or HMVEC-d cells were seeded at ~10% confluence into 96-well plates. After attachment, medium was exchanged for medium containing 1 pmol/L to 1 μmol/L of the indicated protein. Cells were allowed to grow for 7 days and then quantified using CyQUANT (Invitrogen) according to manufacturer's directions. The degree of proliferation in culture was measured by comparing wells in each plate fixed in absolute ethanol on day 0 with experimental wells, with fold proliferation calculated by dividing CyQUANT fluorescence in experimental wells by that in day 0 wells. Groups were compared using Student's *t* test, with Bonferroni correction where appropriate.

HMVEC Trans-well migration assay

Human microvascular endothelial cells were maintained as above. Polycarbonate Transwell inserts, 6.5 mm diameter with 8.0 μm pores, were coated with fibronectin (BD Biosciences). Cells were harvested and resuspended in EBM (Cambrex) containing 0.1% bovine serum albumin (Fisher Chemical). Cells (10,000 per well) were plated onto wells containing medium alone or medium containing the molecule to be tested. These wells were suspended above wells containing 5 to 10 ng/mL recombinant human VEGF (R&D Systems) or full serum medium. Cells were allowed to migrate for 4 h. Membranes were rinsed once in PBS and then fixed and processed using Diff-Quick (Dade Diagnostics). Cells on the top of the membrane were removed using cotton-tipped applicators, and the membrane was removed from the insert using a scalpel. Membranes were then mounted on slides, and the number of cells in a microscopic field was counted manually.

HMVEC CMG2 / TEM8 siRNA knockdown

CMG2 and/or TEM8 knockdown in HMVEC was achieved using Dharmacon smartpools (Dharmacon, Lafayette, CO) and RNAimax (ThermoFisher, Waltham, MA) in OPTI-MEM with Glutamax (ThermoFisher, Waltham, MA). Approximately 6 hours after addition of the transfection complex, an equal volume of EBM-2 was added to the cells, and media was changed to EBM-2 ~18 hours later.

Western Blotting

Near-confluent HMVEC WT and CMG2 / TEM8 KD cells were washed three times in cold PBS and lysed for 30 min at 4°C in PBS supplemented with 1% Triton X-100 and a protease inhibitor cocktail (cOmplete mini protease inhibitor cocktail, Roche). Lysates were cleared by centrifugation at 16,000 xg and the supernatant protein concentration was measured by BCA assay. Protein (40μg) from each sample was used for SDS-PAGE and blotted onto PVDF. Following blocking, the membranes were probed with antibodies against CMG2 (1:1000 16723–1-AP, Proteintech, Rosemont, IL) or TEM8 (1:1000 ab21269, Abcam, Cambridge, UK), then stripped and reprobed for beta-actin (1:10,000 A5441, Sigma) as loading control. Blots were imaged using a ChemiDoc imager (Bio-Rad, Hercules, CA).

HMVEC tube formation assay

Human microvascular endothelial cells were maintained as above. Before the assay, a 1- to 2-mm layer of Matrigel was plated into the wells of a 12-well cluster. Approximately 10^5 cells were plated on this layer in EGM-2. Plates were examined at 12, 14, 16, 18, and 24 h for differences in network formation. In each experiment, good network formation was observed in untreated control wells.

Morphological characterization of of P5 retinal vasculature

Progeny of a het-het cross of CMG2-ΔTM-ICD were collected and euthanized by decapitation. Eyes were dissected from the head using scalper and forceps and fixed in 4% PFA for 30–120 min., then transferred to PBS. Retinas were dissected by removing the cornea and iris, then using forceps to dissect the choroid away from the retina and lens. The lens and then hyaloid vessels were then removed and the retina permeabilized and blocked overnight in 0.5% Triton X-100 and 1% BSA in PBS at 4°C. Retinas were stained with 1:200 FITC-Isolectin B4 (Vector Labs, Burlingame, CA, USA) in PBS containing 1mM CaCl2 for 24–72 hours. After staining, retinas were washed 5× 10 min. in PBS at room temperature. Retinas were then relaxed using four radial cuts and they were mounted under coverslips using SlowFade Gold antifade (ThermoFischer, Burlington, MA, USA). Retinas of $CMG2^{wt}$ and $CMG2^{-/-}$ animals were then imaged under standard illumination and exposure with a Zeiss Axiophot Upright Florescence Microscope in tiling mode (4×4 mosaic from the center of optic nerve) at 5x magnification and measured by an investigator blinded to genotype. Arterial branching was scored using the rubrik in Supplemental File 1.

CMG2 ECM ELISA

All steps were performed at room temperature unless otherwise indicated. For binding assays, matrix protein (Rockland Immunochemicals, Corning, EMD Millipore) was

adsorbed onto 96-well polyethylene plates (Greiner) by incubating 2 ug/mL matrix protein in HBS with 2 mM Mg^{2+} and Ca^{2+} (Buffer A) in individual wells at 4° C overnight. *Bacillus anthracis* protective antigen (PA) was treated similarly but was incubated at 1 μM in the same buffer. After incubation, wells were washed 3x with Buffer A and blocked with 5% BSA (GoldBio) in HBS with 2 mM Mg^{2+}, 2 mM Ca^{2+}, and 0.1% Tween-20 (Buffer B) for 1 hour. Blocking was followed by 3 washes with Buffer B, after which varying concentrations of a biotinylated CMG2-AviTag construct (for matrix, 2.1 μM to 10 nM; for PA, 4 μM to 1 pM) were dissolved in Buffer B and incubated in wells for 4 hours. After incubation with CMG2-AviTag, wells were again washed 3 times, after which streptavidin-HRP (Thermo Scientific) diluted in Buffer B with 5% BSA was incubated in wells for 1 hour. Wells were then washed 6 times with Buffer B, after which 1x TMB solution (Thermo Scientific) was added to wells. Once the color was visible in wells, the reaction was quenched with 0.2 M H2SO4. Wells were read out in a BioTek H4 Hybrid plate reader (BioTek) by quantifying well absorbance at 450 nm. Data were analyzed in Microsoft Excel, and Kd values were calculated in MATLAB using the sigm_fit function.

EA.hy926 cell culture

EA.hy926 (CRL-2922) cells result from a fusion of human umbilical vein cells with lung carcinoma cells. Cells were cultured in 10% FBS + DMEM and incubated at 37°C in a humidified environment with 5% CO_2 until ready for passaging.

EA.hy926 cell proliferation assay

EA.hy926 cells (15,000 per well) were seeded into each well in a 96 well plate and incubated for 1 h to attach. After cell attachment, media with treatments were added. Ethanol fixed cells were used as negative (background) control. After a 24 h incubation, 20 μL CellTiter-Blue Reagent (Promega) was added to each well for 4 h. The fluorescence signal (Ex: 560nm / Em: 590nm) was measured using a BioTek Synergy H2 plate reader. All readings were normalized to the non-treated control.

Cell ASIC gradient migration assay

The assay protocol followed the CellASIC ONIX M04G-02 Microfluidic Gradient Plate User Guide. All media put into the plate (excepting the cell suspension) was filtered through a 0.2 μm syringe filter. EA.hy926 cells (3×10^6 cells/mL) were loaded in and incubated overnight with DMEM + 10% FBS under flow at 37°C. Assays were then performed with a stable DMEM + 0 – 10% FBS gradient with or without treatment. Unless otherwise indicated, microfluidic devices were primed with full-serum media, which will result in serum proteins adsorbing to available surfaces and serving as the migration substrate. Brightfield images at 10x magnification were taken every 10 min over 12 h on an Olympus IX73 microscope and the ORCA-Flash4.0 camera (Hamamatsu). Individual cells were tracked with Image J manual tracking plugin. Data was transferred into the Ibidi Chemotaxis and Migration Tools 2.0. to export the endpoint y-displacement and the accumulated displacement. P-values were calculated using a two-sided Student's *t*-test or ANOVA using the Tukey correction. Error bars represent the standard error of the mean (n=40 cells).

Peptide growth factors (hVEGF165, Gold Biotechnology, St. Louis, MO, USA; human bFGF, Gold Biotechnology, St. Louis, MO, USA; recombinant hPDGF-BB, ThermoFischer, Waltham, MA, USA) and were dissolved in PBS, aliquoted, and stored at −80oC before use, limiting freeze-thaw cycles. C3 (Cytoskeleton, Denver, CO, USA) was dissolved in ddH2O and used according to the manufacturer's instructions. Sphingosine-1-phosphate (S1P, Alabaster, AL, USA) was dissolved in methanol:chloroform and 200 μmoles/tube evaporated to dryness in Eppendorf tubes in a SpeedVac. Dried lipid was then resuspended in 130μl of a solution of 0.4% fatty-acid free albumin (Sigma-Aldrich, St. Louis, MO, USA) in PBS, sonicated in a bath sonicator for 5 minutes, and equilibrated at 4°C overnight to generate a 200μM solution, which was frozen for storage or transportation then thawed and diluted for use, as appropriate.

EA.hy926 CMG2 KO development:

HEK293T cells (3.8×10^6 cells) were seeded in a 10cm tissue culture dish for 18 hours. Then, 12μg of pCMV, 5μg of pVSVG, 12.5μg of Lenti-CRISPR (targeting CMG2 exon 1, sgRNA sequence: GCACCAACAGCCACAGCCCG), 90μL of 1mg/mL PEI and 600μL of serum-free DMEM were mixed into a tube and incubated for 15 minutes before adding to the 10cm culture dish. The dish was replaced with 10mL of 10% FBS DMEM in 4 hours and followed by 48 hours incubation. The media was removed from the transfected cells into a conical tube, which was spin at 2500g for 3 minutes to remove debris. The supernatant (lentivirus) and 10μg/mL polybrene were added to 40% confluent EA.hy926 cells and incubated for 24 hours. The next day, media was removed, fresh 10% FBS DMEM and 1μg/mL puromycin were added to the plate for 3–5 days. After 3–5 days, the cells that survived in the selection were diluted into single colonies in a 96-well plate.

PA uptake flow cytometry:

CMG2 KO EA.hy 926 cells and WT EA.hy926 cells were plated in a 12-well plate at 50% confluence. Next, a PA-Alexa Fluor 546 conjugate was added into each well at the CMG2 K_d (200pM) and incubated overnight at 37°C. The next day, cells were trypsinized and resuspended into a microcentrifuge tube. Cells were washed once with complete media, and 50,000 cells were resuspended in complete media. Triplicate samples (three samples for each condition +/− PA-AlexaFluor 546) were analyzed using a Beckman-Coulter Cytoflex using the 488 nm laser for excitation. Data were analyzed using FlowJo software. Singlets were gated using forward scatter-height vs. forward scatter-area, and the median fluorescence intensity (MFI) was determined for each sample in the appropriate fluorescence channel.

CMG2-Clover add-back vector

A lentiviral transfer vector, pLJM1-$CMG2^{488}$-Clover, was constructed by generating a PCR fragment containing the $CMG2^{488}$ ORF flanked by HindIII and EcoRI sites using the primers ATAAAGCTTATGGTGGCGGAGC and ATACCGAATTCCTGAGATGGAACT and $pLEGFP^{488}$ [44] (a kind gift of John Young) as template. This fragment was ligated into pcDNA3-Clover [45] (a gift from Michael Lin; Addgene plasmid # 40259) and this was then used as template to generate a PCR fragment coding for $CMG2^{488}$-Clover flanked by AgeI and SalI sites using the primers ATATATACCGGTCCCAAGCTTATGGTGGCG

and ATATATGTCGACTCTAGCATTTAGGTGACACTATAGAATAGG. This fragment was cloned into pLJM1 [46] (a gift from Richard Possemato; Addgene plasmid # 164143) using AgeI and SalI. The resulting vector codes for a fusion protein with sequence CMG2^{488}-EFY-Clover-SRGPYSIVSPKC. The sequence of the insert in the final construct was verified by Sanger sequencing.

Adhesion assay

EA.hy926 cells were grown in DMEM supplemented with 10% FBS. 20μg/mL collagen I, IV, VI, laminin, fibronectin, PA^{SSSR}, and BSA were prepared in PBS and coated on 96 well plates (100 μg/well) overnight at 4°C. After coating, collagen I, IV, VI, laminin, fibronectin, PA^{SSSR}, and BSA were removed, and wells were blocked with 5% BSA for 1 hour. Cells were serum-starved and harvested by scraping, then centrifuging at 100xg for 10 minutes; the supernatant was discarded. Cells were then resuspended at 2–3×10^5 cells/mL in DMEM. 100μL of cells were added to each of the coated wells. The plate was incubated at 37°C for 1 hour to allow the cells to adhere to the surface. Each well was washed gently twice using warm serum-free DMEM, then 100μL of serum-free DMEM and 20μL of Cell-Titer Blue (Promega) were added into each well, and plates were incubated at 37°C. After 4 hours of incubation, the fluorescence signal from the 96 well plate was measured at (Ex: 560nm / Em: 590nm).

Supplementary Material

Refer to Web version on PubMed Central for supplementary material.

Acknowledgements/Sources of Funding:

The CMG2-Fc and TEM8-Fc fusion proteins were a kind gift of Planet Biotechnology. The SR-8F7/C7 anti-CMG2 antibody and associated data were a kind gift of Gisou van der Goot and Laurence Abrami. The L2 anti-TEM8 antibody was a kind gift of Brad St. Croix. Funding was provided by the NEI (R01EY018829), NINDS (R21NS059411), and DOD CDMRP (W81XWH-08-1-0710).

Data Availability:

The datasets generated during and/or analyzed during the current study are available from the corresponding author on reasonable request.

References:

1. Folkman J (2007) Angiogenesis: an organizing principle for drug discovery? Nat Rev Drug Discov 6 (4):273–286. doi:nrd2115 [pii] 10.1038/nrd2115 [PubMed: 17396134]
2. Blanco R, Gerhardt H (2013) VEGF and Notch in tip and stalk cell selection. Cold Spring Harb Perspect Med 3 (1):a006569. doi:10.1101/cshperspect.a006569 [PubMed: 23085847]
3. Kretschmer M, Rudiger D, Zahler S (2021) Mechanical Aspects of Angiogenesis. Cancers (Basel) 13 (19). doi:10.3390/cancers13194987
4. Rogers MS, Christensen KA, Birsner AE, Short SM, Wigelsworth DJ, Collier RJ, D'Amato RJ (2007) Mutant anthrax toxin B moiety (protective antigen) inhibits angiogenesis and tumor growth. Cancer Res 67 (20):9980–9985. doi:10.1158/0008-5472.CAN-07-0829 [PubMed: 17942931]
5. Moayeri M, Wiggins JF, Leppla SH (2007) Anthrax protective antigen cleavage and clearance from the blood of mice and rats. Infect Immun 75 (11):5175–5184. doi:IAI.00719–07 [pii] 10.1128/IAI.00719-07 [PubMed: 17724066]

6. Wigelsworth DJ, Krantz BA, Christensen KA, Lacy DB, Juris SJ, Collier RJ (2004) Binding stoichiometry and kinetics of the interaction of a human anthrax toxin receptor, CMG2, with protective antigen. J Biol Chem 279 (22):23349–23356 [PubMed: 15044490]
7. Liu S, Crown D, Miller-Randolph S, Moayeri M, Wang H, Hu H, Morley T, Leppla SH (2009) Capillary morphogenesis protein-2 is the major receptor mediating lethality of anthrax toxin in vivo. Proc Natl Acad Sci U S A 106 (30):12424–12429 [PubMed: 19617532]
8. Jia Z, Ackroyd C, Han T, Agrawal V, Liu Y, Christensen K, Dominy B (2017) Effects from metal ion in tumor endothelial marker 8 and anthrax protective antigen: BioLayer Interferometry experiment and molecular dynamics simulation study. J Comput Chem 38 (15):1183–1190. doi:10.1002/jcc.24768 [PubMed: 28437008]
9. Bradley KA, Mogridge J, Mourez M, Collier RJ, Young JAT (2001) Identification of the cellular receptor for anthrax toxin. Nature 414 (6860):225–229. doi:DOI 10.1038/n35101999 [PubMed: 11700562]
10. Wigelsworth DJ, Krantz BA, Christensen KA, Lacy DB, Juris SJ, Collier RJ (2004) Binding stoichiometry and kinetics of the interaction of a human anthrax toxin receptor, CMG2, with protective antigen. J Biol Chem 279 (22):23349–23356. doi:10.1074/jbc.M401292200 [PubMed: 15044490]
11. Liu S, Zhang Y, Hoover B, Leppla SH (2012) The receptors that mediate the direct lethality of anthrax toxin. Toxins (Basel) 5 (1):1–8. doi:10.3390/toxins5010001 [PubMed: 23271637]
12. Wycoff K, Maclean J, Belle A, Yu L, Tran Y, Roy C, Hayden F (2015) Anti-infective immunoadhesins from plants. Plant Biotechnol J 13 (8):1078–1093. doi:10.1111/pbi.12441 [PubMed: 26242703]
13. Wycoff KL, Belle A, Deppe D, Schaefer L, Maclean JM, Haase S, Trilling AK, Liu S, Leppla SH, Geren IN, Pawlik J, Peterson JW (2011) Recombinant anthrax toxin receptor-Fc fusion proteins produced in plants protect rabbits against inhalational anthrax. Antimicrob Agents Chemother 55 (1):132–139. doi:10.1128/AAC.00592-10 [PubMed: 20956592]
14. Burgi J, Kunz B, Abrami L, Deuquet J, Piersigilli A, Scholl-Burgi S, Lausch E, Unger S, Superti-Furga A, Bonaldo P, van der Goot FG (2017) CMG2/ANTXR2 regulates extracellular collagen VI which accumulates in hyaline fibromatosis syndrome. Nat Commun 8:15861. doi:10.1038/ncomms15861 [PubMed: 28604699]
15. Chaudhary A, Hilton MB, Seaman S, Haines DC, Stevenson S, Lemotte PK, Tschantz WR, Zhang XM, Saha S, Fleming T, St Croix B (2012) TEM8/ANTXR1 Blockade Inhibits Pathological Angiogenesis and Potentiates Tumoricidal Responses against Multiple Cancer Types. Cancer Cell 21 (2):212–226. doi:S1535–6108(12)00037–2 [pii] 10.1016/j.ccr.2012.01.004 [PubMed: 22340594]
16. Reeves CV, Dufraine J, Young JA, Kitajewski J (2010) Anthrax toxin receptor 2 is expressed in murine and tumor vasculature and functions in endothelial proliferation and morphogenesis. Oncogene 29 (6):789–801 [PubMed: 19901963]
17. Peters DE, Zhang Y, Molinolo AA, Miller-Randolph S, Szabo R, Bugge TH, Leppla SH, Liu S (2012) Capillary morphogenesis protein-2 is required for mouse parturition by maintaining uterine collagen homeostasis. Biochem Biophys Res Commun 422 (3):393–397. doi:10.1016/j.bbrc.2012.04.160 S0006–291X(12)00849–2 [pii] [PubMed: 22575514]
18. Cryan LM, Bazinet L, Habeshian KA, Cao S, Clardy J, Christensen KA, Rogers MS (2013) 1,2,3,4,6-Penta-O-galloyl-beta-d-glucopyranose Inhibits Angiogenesis via Inhibition of Capillary Morphogenesis Gene 2. J Med Chem 56 (5):1940–1945. doi:10.1021/jm301558t [PubMed: 23394144]
19. E GD, Carrero P, Madrona A, Rodriguez-Salamanca P, Martinez-Gualda B, Camarasa MJ, Jimeno ML, Bennallack PR, Finnell JG, Tsang TM, Christensen KA, San-Felix A, Rogers MS (2019) Galloyl Carbohydrates with Antiangiogenic Activity Mediated by Capillary Morphogenesis Gene 2 (CMG2) Protein Binding. J Med Chem 62 (8):3958–3970. doi:10.1021/acs.jmedchem.8b01988 [PubMed: 30964669]
20. Finnell JG, Tsang TM, Cryan L, Garrard S, Lee SL, Ackroyd PC, Rogers MS, Christensen KA (2020) A Canstatin-Derived Peptide Provides Insight into the Role of Capillary Morphogenesis Gene 2 in Angiogenic Regulation and Matrix Uptake. ACS Chem Biol 15 (2):587–596. doi:10.1021/acschembio.0c00064 [PubMed: 32003961]

21. Rogers MS, Cryan LM, Habeshian KA, Bazinet L, Caldwell TP, Ackroyd PC, Christensen KA (2012) A FRET-based high throughput screening assay to identify inhibitors of anthrax protective antigen binding to capillary morphogenesis gene 2 protein. PLoS One 7 (6):e39911. doi:10.1371/journal.pone.0039911 10-PONE-RA-21353 [pii] [PubMed: 22768167]
22. Cao S, Cryan L, Habeshian KA, Murillo C, Tamayo-Castillo G, Rogers MS, Clardy J (2012) Phenolic compounds as antiangiogenic CMG2 inhibitors from Costa Rican endophytic fungi. Bioorg Med Chem Lett 22 (18):5885–5888. doi:10.1016/j.bmcl.2012.07.075 S0960–894X(12)00960–2 [pii] [PubMed: 22910038]
23. Lacy DB, Wigelsworth DJ, Scobie HM, Young JAT, Collier RJ (2004) Crystal structure of the von Willebrand factor A domain of human capillary morphogenesis protein 2: An anthrax toxin receptor. P Natl Acad Sci USA 101 (17):6367–6372. doi:10.1073/pnas.0401506101
24. Whittaker CA, Hynes RO (2002) Distribution and evolution of von Willebrand/integrin A domains: widely dispersed domains with roles in cell adhesion and elsewhere. Mol Biol Cell 13 (10):3369–3387. doi:10.1091/mbc.E02-05-0259 [PubMed: 12388743]
25. Gao M, Schulten K (2006) Onset of anthrax toxin pore formation. Biophys J 90 (9):3267–3279. doi:10.1529/biophysj.105.079376 [PubMed: 16473908]
26. Scobie HM, Rainey GJA, Bradley KA, Young JAT (2003) Human capillary morphogenesis protein 2 functions as an anthrax toxin receptor. P Natl Acad Sci USA 100 (9):5170–5174. doi:10.1073/pnas.0431098100
27. Bell SE, Mavila A, Salazar R, Bayless KJ, Kanagala S, Maxwell SA, Davis GE (2001) Differential gene expression during capillary morphogenesis in 3D collagen matrices: regulated expression of genes involved in basement membrane matrix assembly, cell cycle progression, cellular differentiation and G-protein signaling. J Cell Sci 114 (Pt 15):2755–2773 [PubMed: 11683410]
28. Cryan LM, Habeshian KA, Caldwell TP, Morris MT, Ackroyd PC, Christensen KA, Rogers MS (2013) Identification of Small Molecules That Inhibit the Interaction of TEM8 with Anthrax Protective Antigen Using a FRET Assay. J Biomol Screen 18 (6):714–725. doi:1087057113478655 [pii] 10.1177/1087057113478655 [PubMed: 23479355]
29. Vink JY, Charles-Horvath PC, Kitajewski JK, Reeves CV (2014) Anthrax toxin receptor 2 promotes human uterine smooth muscle cell viability, migration and contractility. Am J Obstet Gynecol 210 (2):154 e151–158. doi:10.1016/j.ajog.2013.09.030 [PubMed: 24060446]
30. Lawson CD, Ridley AJ (2018) Rho GTPase signaling complexes in cell migration and invasion. J Cell Biol 217 (2):447–457. doi:10.1083/jcb.201612069 [PubMed: 29233866]
31. Narumiya S, Tanji M, Ishizaki T (2009) Rho signaling, ROCK and mDia1, in transformation, metastasis and invasion. Cancer Metast Rev 28 (1–2):65–76. doi:10.1007/s10555-008-9170-7
32. Castanon I, Abrami L, Holtzer L, Heisenberg CP, van der Goot FG, Gonzalez-Gaitan M (2013) Anthrax toxin receptor 2a controls mitotic spindle positioning. Nat Cell Biol 15 (1):28–39. doi:10.1038/ncb2632 [PubMed: 23201782]
33. Jérôme Bürgi LA, Castanon Irinka, Yan Shixu E., Luciano A, Abriata ML, Unger Sheila, Superti-Furga Andrea, Dal Peraro Matteo, MGGaFGvd Goot (2019) A Novel talin-to-RhoA switch mechanism upon ligand binding of the collagen VI receptor CMG2. Developmental Cell
34. Zahra FT, Sajib MS, Ichiyama Y, Akwii RG, Tullar PE, Cobos C, Minchew SA, Doci CL, Zheng Y, Kubota Y, Gutkind JS, Mikelis CM (2019) Endothelial RhoA GTPase is essential for in vitro endothelial functions but dispensable for physiological in vivo angiogenesis. Sci Rep 9 (1):11666. doi:10.1038/s41598-019-48053-z [PubMed: 31406143]
35. Burgi J, Abrami L, Castanon I, Abriata LA, Kunz B, Yan SE, Lera M, Unger S, Superti-Furga A, Peraro MD, Gaitan MG, van der Goot FG (2020) Ligand Binding to the Collagen VI Receptor Triggers a Talin-to-RhoA Switch that Regulates Receptor Endocytosis. Dev Cell 53 (4):418–430 e414. doi:10.1016/j.devcel.2020.04.015 [PubMed: 32428455]
36. Bayless KJ, Johnson GA (2011) Role of the cytoskeleton in formation and maintenance of angiogenic sprouts. J Vasc Res 48 (5):369–385. doi:10.1159/000324751 [PubMed: 21464572]
37. Martin M, Veloso A, Wu J, Katrukha EA, Akhmanova A (2018) Control of endothelial cell polarity and sprouting angiogenesis by non-centrosomal microtubules. Elife 7. doi:10.7554/eLife.33864

38. Welti JC, Gourlaouen M, Powles T, Kudahetti SC, Wilson P, Berney DM, Reynolds AR (2011) Fibroblast growth factor 2 regulates endothelial cell sensitivity to sunitinib. Oncogene 30 (10):1183–1193. doi:10.1038/onc.2010.503 [PubMed: 21057538]

39. Casanovas O, Hicklin DJ, Bergers G, Hanahan D (2005) Drug resistance by evasion of antiangiogenic targeting of VEGF signaling in late-stage pancreatic islet tumors. Cancer Cell 8 (4):299–309. doi:10.1016/j.ccr.2005.09.005 [PubMed: 16226705]

40. Huang D, Ding Y, Zhou M, Rini BI, Petillo D, Qian CN, Kahnoski R, Futreal PA, Furge KA, Teh BT (2010) Interleukin-8 mediates resistance to antiangiogenic agent sunitinib in renal cell carcinoma. Cancer Res 70 (3):1063–1071. doi:10.1158/0008-5472.CAN-09-3965 [PubMed: 20103651]

41. Porta C, Paglino C, Imarisio I, Ganini C, Sacchi L, Quaglini S, Giunta V, De Amici M (2013) Changes in circulating pro-angiogenic cytokines, other than VEGF, before progression to sunitinib therapy in advanced renal cell carcinoma patients. Oncology 84 (2):115–122. doi:10.1159/000342099 [PubMed: 23154434]

42. Friedlander M (2009) Combination angiostatic therapies: targeting multiple angiogenic pathways. Retina 29 (6 Suppl):S27–29. doi:10.1097/IAE.0b013e3181ad2673 [PubMed: 19553794]

43. Rogers MS, Birsner AE, D'Amato RJ (2007) The mouse cornea micropocket angiogenesis assay. Nat Protoc 2 (10):2545–2550 [PubMed: 17947997]

44. Scobie HM, Rainey GJ, Bradley KA, Young JA (2003) Human capillary morphogenesis protein 2 functions as an anthrax toxin receptor. Proc Natl Acad Sci U S A 100 (9):5170–5174 [PubMed: 12700348]

45. Lam AJ, St-Pierre F, Gong Y, Marshall JD, Cranfill PJ, Baird MA, McKeown MR, Wiedenmann J, Davidson MW, Schnitzer MJ, Tsien RY, Lin MZ (2012) Improving FRET dynamic range with bright green and red fluorescent proteins. Nat Methods 9 (10):1005–1012. doi:10.1038/nmeth.2171 nmeth.2171 [pii] [PubMed: 22961245]

46. Golden RJ, Chen B, Li T, Braun J, Manjunath H, Chen X, Wu J, Schmid V, Chang TC, Kopp F, Ramirez-Martinez A, Tagliabracci VS, Chen ZJ, Xie Y, Mendell JT (2017) An Argonaute phosphorylation cycle promotes microRNA-mediated silencing. Nature 542 (7640):197–202. doi:10.1038/nature21025 [PubMed: 28114302]

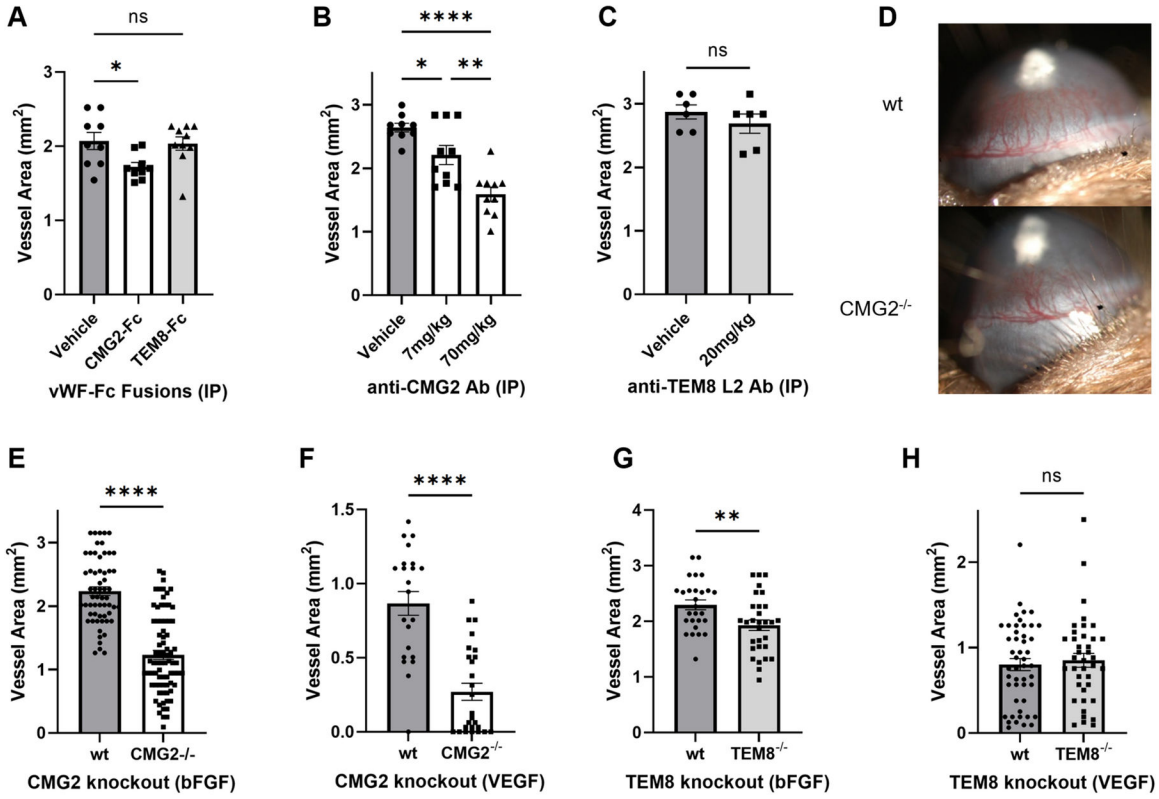

Figure 1. Blocking the interactions of CMG2 with its natural ligand inhibits both FGF and VEGF induced corneal neovascularization *in vivo*.

(A) Corneal micropocket assay on mice treated with soluble ECD of either CMG2 or TEM8, via intraperitoneal injection. (n=9, 9, 10 eyes) (B-C) Corneal micro-pocket assay on mice treated with either anti-CMG2 SR-8F7/C7 antibody (B, n=9, 10, 10 eyes) or anti-TEM8 L2 antibody (C, n=6, 6 eyes) on days 1 and 3 at the indicated dose. Corneal neovascularization in these assays was induced by bFGF before treatment; vessel area on both the left and right corneas were measured from each mouse. (D) Representative image of corneal neovascularization in both wild type (WT) and CMG2 −/− male mice. (E-F) Comparison of corneal neovascularization between WT and CMG2−/− mice induced by either bFGF (E, n=59, 76 eyes) or VEGF (F, n=22, 26 eyes). CMG2−/− mice showed significant reductions in neovascularization for both bFGF- and VEGF-induced angiogenesis. (G-H) A similar experiment was performed with WT and TEM8−/− mice with either bFGF (G, n=27, 30 eyes) or VEGF (H, n=48, 39 eyes). Data presented are pooled from both sexes. Error bars are standard error of mean, * $p<0.05$; ** $p<0.01$; *** $p<0.001$; **** $p<0.001$ by two-sided Student's *t*-test for C, E, F, G, and H, and by ANOVA with Tukey's post-test for A and B. The measuring investigator was blind to treatment groups and genotype.

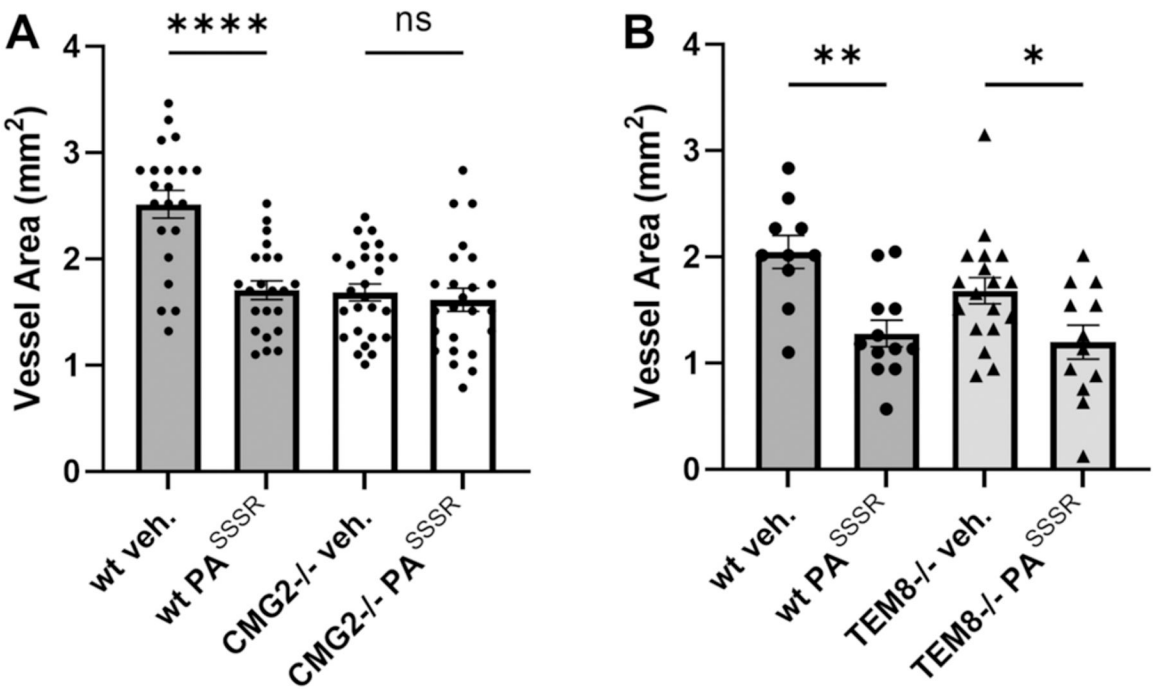

Figure 2. CMG2 is the primary receptor that mediates PA^{SSSR}-induced inhibition of angiogenesis.

(A) Comparative levels of bFGF-induced corneal neovascularization between CMG2−/− and WT mice treated with or without PA^{SSSR} (n=21, 22, 26, 24 eyes), and (B) TEM8−/− and WT mice treated with or without PA^{SSSR} (n=10, 12, 18, 12 eyes). Results showed that PA^{SSSR} reduced vessel formation on TEM8−/− mice but not CMG2−/− mice. Error bars are standard error of mean. Data are pooled from both sexes. Error bars are standard error of mean, * $p<0.05$; ** $p<0.01$; **** $p<0.001$ by ANOVA with Tukey's post-test. The measuring investigator was blind to treatment groups and genotype in all experiments.

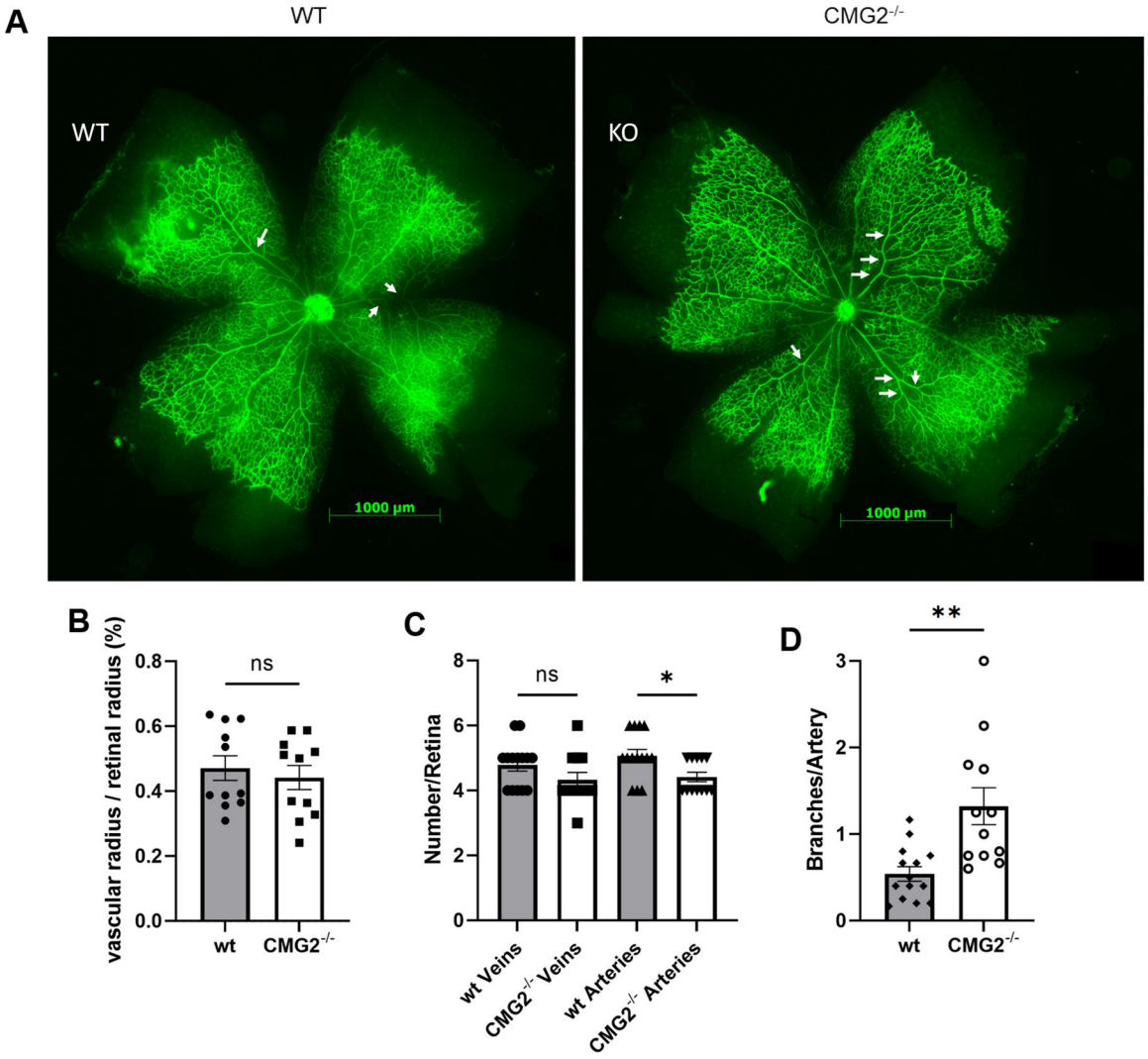

Figure 3. CMG2 KO increases vessel branching in the mouse retina.

(A) Representative mages of vessel formation in the retina of both WT (left) and CMG2−/− (right) mice. Arteriolar branches are indicated by arrowheads. (B-D) Quantified vessel formation from retinal assays. (B) Comparison of vascular radius, normalized to the retinal radius, between WT and CMG2−/− mice. n=11, 11 (C) Quantification of arterial branching in both WT and CMG2−/− mouse retinas. n=14, 12 (D) Artery and vein counts per retina as in WT and CMG2−/− mice. CMG2−/− mouse retinas exhibit fewer veins and arteries than WT, but only artery count is significantly lower than WT mice. n=14, 12. Data presented are pooled from both sexes. Error bars are standard error of mean, * $p<0.05$; ** $p<0.01$ by two-sided Student's *t*-test. The measuring investigator was blind to genotype.

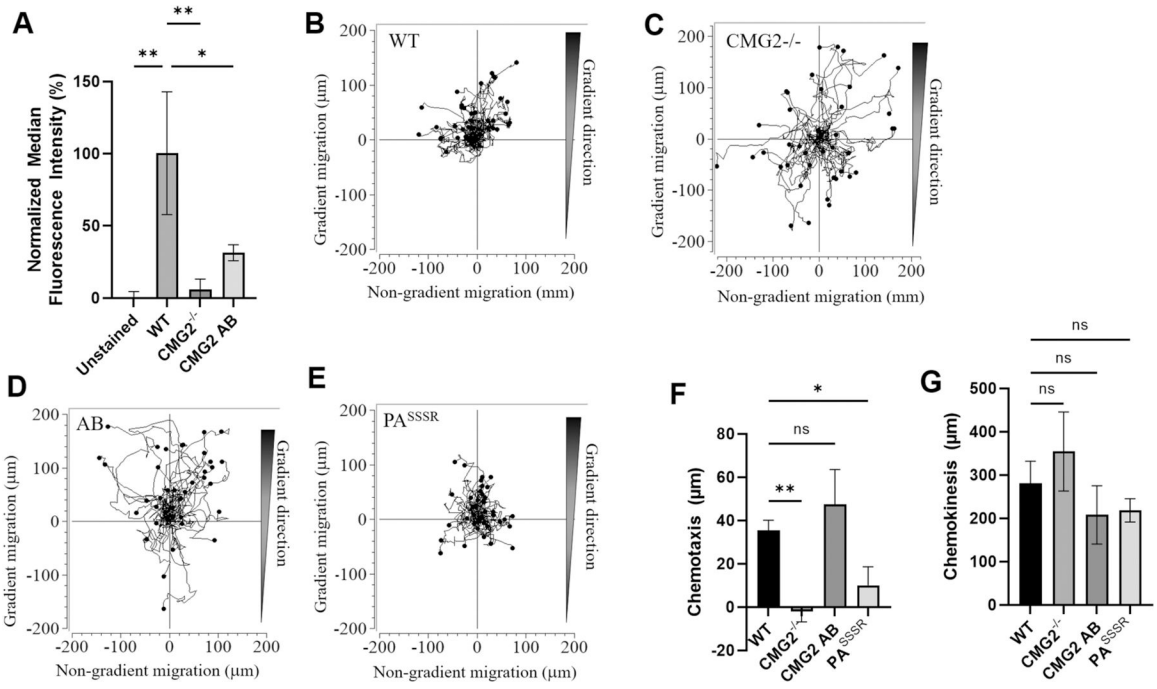

Figure 4. PA^{SSSR} treated and CMG2 KO EA.hy926 endothelial cells lose the ability to migrate toward a serum gradient.

(A) Differential PA-AF586 conjugate uptake by wild type (WT), CMG2-ΔTM-ICD (CMG2$^{-/-}$), and CMG2 add back (AB, CMG2$^{-/-}$ cells transduced with a CMG2 expression vector), EA.hy926 cells via flow cytometry (10,000 cells per condition). Median fluorescence intensity of each condition was normalized against WT signal after subtracting the median fluorescence of the unstained control. Error bars are the standard deviations from three distinct or biological replicates. (B-E) Representative track plots of individual EA.hy926 cells migrating toward serum on serum-treated plates are shown for wild type (WT), CMG2 add back (AB), CMG2-ΔTM-ICD (CMG2$^{-/-}$); and WT with 200pM PA^{SSSR} (PA^{SSSR}). (F-G) Quantification of EA.hy926 chemotaxis (F, displacement toward gradient) and chemokinesis (G, total distance traveled) in the gradient migration assay. For all migration assays, migrating cells were tracked for 8 hours (n=40 cells, 3 biological replicates per condition) using ImageJ and further quantified using the Chemotaxis and Migration Tool (ibidi.com). Error bars represent the standard deviation. ANOVA (A, and F; Dunnett's post test) was used to compare the tested conditions. * $p<0.05$; ** $p<0.01$; ns not significant.

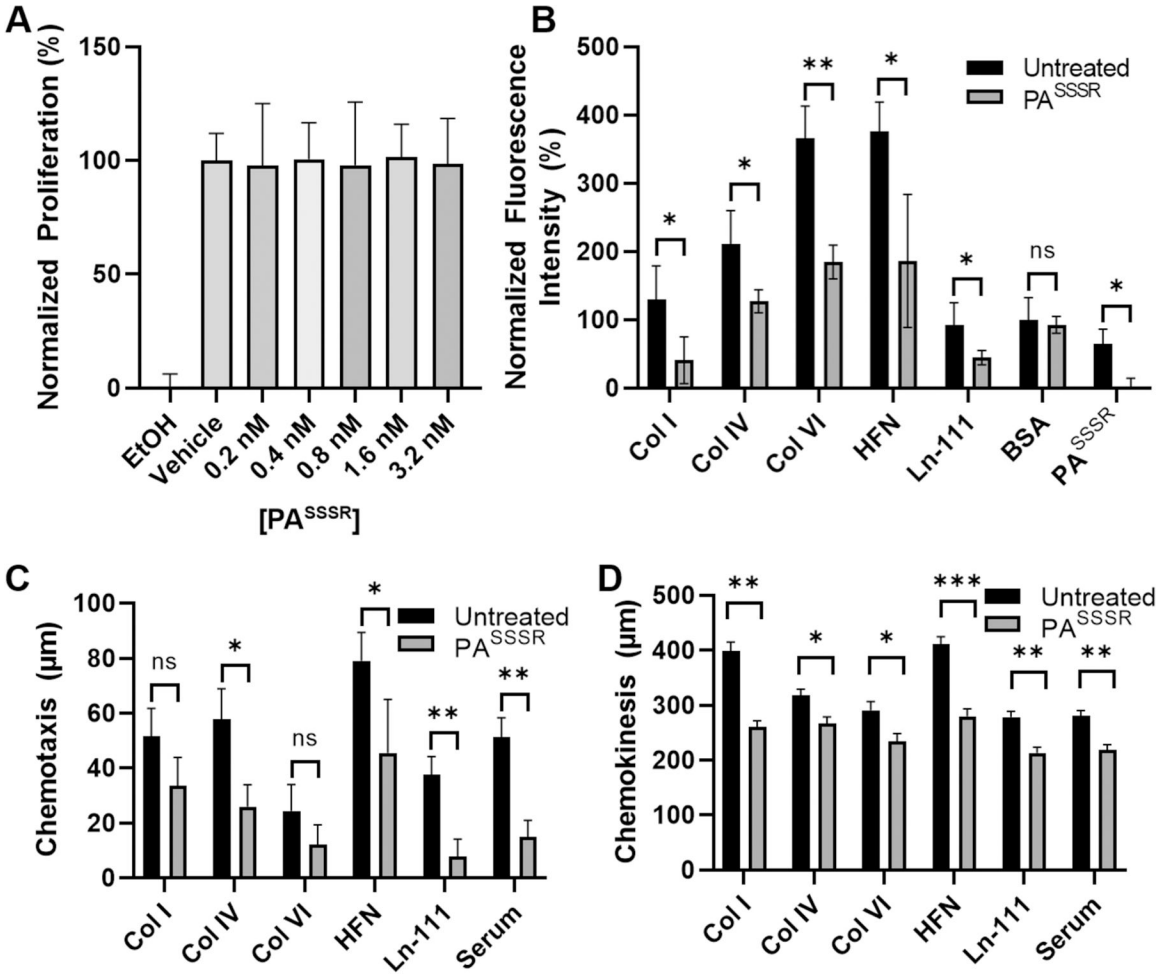

Figure 5. Matrix binding to CMG2 impacts cell adhesion and migration.

(A) EA.hy926 endothelial cell proliferation in different concentrations of PA^{SSSR}. Ethanol (EtOH) treated cells was used as the negative control. Error bars represent the standard deviation (3 distinct samples per concentration). (B) EA.hy926 endothelial cell adhesion to plates coated with various matrix proteins, or no ECM proteins ("BSA"), both with and without addition of the CMG2 antagonist PA^{SSSR} (200 pM). Addition of PA^{SSSR} significantly inhibits adhesion to matrix-coated plates. Adhesion to uncoated plates was not affected by PA^{SSSR} treatment. Error bars represent the standard deviation (n=3 wells as technical replicates for each condition and n=3 biological replicates). A Student's t-test (two-sided) was used to compare the effects of PA^{SSSR} treatment. (C-D) EA.hy926 migration on different ECM coated surfaces compared to a 200 pM PA^{SSSR} treatment. Chemotaxis (C) reflects displacement of individual cells in the direction of the serum gradient while chemokinesis (D) reflects total distance cell traveled, regardless of direction (D). For all experiments, cells (n=40, 3 biological replicates) were tracked for 8 hours using ImageJ and further quantified using the Chemotaxis and Migration Tool (ibidi.com). Statistical significance between untreated and PA^{SSSR} treated cells was calculated using the Student's t-test (two-sided) . Error bars represent the standard deviation. For all panels, * $p<0.05$; ** $p<0.01$; n.s not significant.

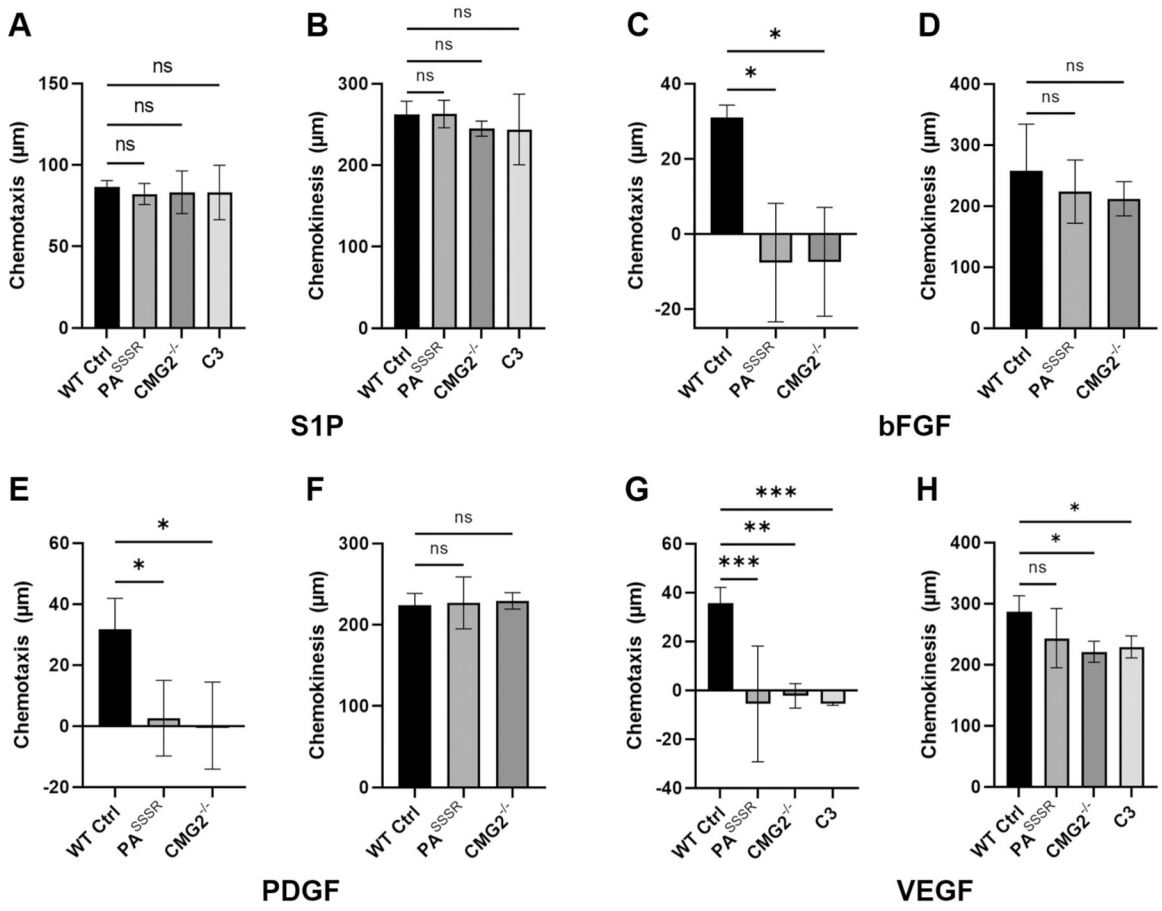

Figure 6. CMG2 and RhoA have a role in growth factor-induced chemotaxis but not S1P-induced chemotaxis.

Quantified chemotaxis (A,C,E,G) and chemokinesis (B,D,F,H) towards various chemoattractants between wild type cells (WT), wild type cells treated with 200 pM PA^{SSSR}, CMG2 knockout ($CMG2^{-/-}$) cells, and wild type cells treated with C3 toxin (1 μg/ml), a RhoA inhibitor. No difference was observed between the different cells under S1P stimulation (A,B). Significantly reduced chemotaxis was observed with PA^{SSSR} treatment and CMG2 knockout cells when stimulated with bFGF, VEGF, and PDGF (C,E,G). EA.hy926 WT cells treated with C3 toxin, a RhoA inhibitor, reduced chemotaxis towards VEGF (G) but not S1P (A). For all migration assays, migrating cells were tracked for 8 hours (n=40 cells, 3 biological replicates per condition) using ImageJ and further quantified using the Chemotaxis and Migration Tool (ibidi.com). Error bars represent the standard deviation. ANOVA with Dunnett's post-test was used to compare the tested conditions. * $p<0.05$; ** $p<0.01$; *** $p<0.001$; ns not significant.

Table 1.

CMG2 binds several broadly expressed matrix proteins with high affinity.

Results of an ELISA-based quantification of CMG2 binding to several broadly expressed matrix proteins, including collagens, laminin-111, and fibronectin. For positive control, PA was assayed for binding to CMG2. Such similar affinities between matrix proteins indicate that CMG2 shows no preference for binding to any one of the matrix proteins assayed.

Protein	K_D (nM)	Std. Dev	Replicates
Collagen I	500	141	3
Collagen VI	800	411	3
Laminin-111	500	158	2
Fibronectin	500	141	3
PA (positive control)	0.46	0.047	3
PA w/EDTA (neg. control)	None	N/A	2

Table 2.

Effects on migration *ex vivo* predict angiogenic effects *in vivo*.

An analysis of the correlation between inhibition of migration *ex vivo* and inhibition of angiogenesis *in vivo*. Compounds identified in a screen as potential CMG2 inhibitors (26 total) were evaluated for effects on HMVEC-d migration (26) and effects on the corneal micropocket assay (19). Compounds that inhibited transwell migration in a screening and second, confirmatory IC50 measurement are considered to affect migration. Similarly, compounds that affected angiogenesis in both a screening and a confirmatory corneal micropocket assay are considered to affect angiogenesis.

	Affects Angiogenesis	**No Effect *In vivo***
Affects migration	6*	2
No effect on migration	1	10

* Includes one compound that stimulated, rather than inhibited, HMVEC migration and increased vessel growth in the cornea. P=0.0033 (χ^2 test).